Three-dimensional multilayered fibrous constructs for wound healing applications

HHS Public Access

Author manuscript

Biomater Sci. Author manuscript; available in PMC 2016 January 27.

Published in final edited form as:

Biomater Sci. 2016 January 26; 4(2): 319–330. doi:10.1039/c5bm00211g.

Three-Dimensional Multilayered Fibrous Constructs for Wound Healing Applications

Tiago C. Reis[a,b], **Steven Castleberry**[b], **Ana M. B. Rego**[c], **Ana Aguiar-Ricardo**[a], and **Paula T. Hammond**[b]

Ana Aguiar-Ricardo: air@fct.unl.pt; Paula T. Hammond: hammond@mit.edu

[a]LAQV, REQUIMTE, Departamento de Química, Faculdade de Ciências e Tecnologia, Universidade Nova de Lisboa, 2829-516 Caparica, Portugal

[b]Department of Chemical Engineering, Massachusetts Institute of Technology, 77 Massachusetts Avenue, Cambridge, MA 02139, USA

[c]CQFM and IN, Instituto Superior Técnico, Universidade de Lisboa, 1049-001 Lisboa, Portugal

Abstract

Electrospun materials are promising scaffolds due to their light-weight, high surface-area and low-cost fabrication, however, such scaffolds are commonly obtained as ultrathin two-dimensional non-woven meshes, lacking on topographical specificity and surface side-dependent properties. Herein, it is reported the production of three-dimensional fibrous materials with an asymmetrical inner structure and engineered surfaces. The manufactured constructs evidence fibrous-based microsized conical protrusions [length: $(9.5 \pm 2.9)\times10^2$ μm; width: $(3.8 \pm 0.8)\times10^2$ μm] at their top side, with a median peak density of 73 peaks.cm^{-2}, while their bottom side resembles to a non-woven mesh commonly observed in the fabrication of two-dimensional electrospun materials. Regarding their thickness (3.7 ± 0.1 mm) and asymmetric fibrous inner architecture, such materials avoid external liquid absorption while promoting internal liquid uptake. Nevertheless, such constructs also observed the high porosity (89.9%) and surface area (1.44 m^2.g^{-1}) characteristic of traditional electrospun mats. Spray layer-by-layer assembly is used to effectively coat the structurally complex materials, allowing to complementary tailor features such water vapor transmission, swelling ratio and bioactive agent release. Tested as wound dressings, the novel constructs are capable of withstanding $(11.0 \pm 0.3)\times10^4$ kg.m^{-2} even after 14 days of hydration, while actively promote wound healing (90 ± 0.5 % of wound closure within 48 hours) although avoiding cell adhesion on the dressings for a painless removal.

Keywords

three-dimensionality; surface design; layer-by-layer; electrospinning; wound dressing

Correspondence to: Ana Aguiar-Ricardo, air@fct.unl.pt; Paula T. Hammond, hammond@mit.edu.

†Electronic Supplementary Information (ESI) available: See: DOI: 10.1039/x0xx00000x

Introduction

The importance of construct topography in applications ranging from anisotropic wetting[1] and antireflection[2] to stem cell differentiation[3, 4] and tissue engineering,[5] has driven multidisciplinary teams to develop a number of novel scaffolds fabrication methods.[6–9] Electrospinning is a versatile means of producing nano- and micro-sized fibers to assemble materials with controlled orientation and fiber density,[10–12] being currently developed towards new methods to enhance yield and the rate of fabrication.[13] However, even the current electrospinning-based approaches have only been used to create two-dimensional electrospun constructs (2DECs). The promising combination of controlled three-dimensional topography, with the existing benefits of electrospun scaffolds, offers new opportunities for the production of fibrous materials with superior structural and surface properties. Three-dimensional electrospun constructs (3DECs) with tailored topographies can be obtained by either post-construction modification or assembly-based mechanisms. The former consists in the use of independent techniques to alter the as-spun materials, such as modulated femtosecond laser pulses[14] or photopatterning.[15] Such methods rely on surface ablation or sacrificial removal of construct material, a strategy that is undesirable when spinning high-value and perishable materials. Controlling topography via process-based assembly mechanisms, in contrast, harnesses the electrostatic forces used to guide the fiber deposition, by either using tailored grounded collectors or by inducing the self-organization of fibers.[16] Self-organization also has the unique feature of allowing for z-axis asymmetric fiber deposition, wherein the bottom and top sides of the same scaffold can show different structural features (e.g. fiber alignment, pore size, etc.). The bottom side of the construct is commonly composed of randomly distributed fibers, similar to the case of many 2D non-woven electrospun meshes, and the materials top side can be tuned into fibrous macro-assembled structures such as stacks,[17, 18] honey-comb patterns[19, 20] or yarns.[21] We have previously described the mechanism underlying this microstructuring process as a result of the *in situ* polarization of collected fibers due to the strong electric field applied, favoring the continuous electrostatic attraction of incoming fibers to specific regions.[22] The use of strong electric fields for electrospinning polymer blends or doped solutions however, causes charged species within the material to separate due to electrophoretic phenomena,[21, 23] driving the anionic elements to the outer surface of the fiber. This process causes poor intermolecular blending, which affects mechanical strength,[24] electrical conductivity[25] and drug release profiles.[26] Thus, the process conditions used to induce the assembly of structures constrain the potential of 3DECs in several applications, especially in cases where incorporation of charged elements is desired.

Layer-by-layer (LbL) assembly technique is a simple and robust method for the incorporation of material into ultra-thin polymer coatings which has been used for applications ranging from surface modification to drug delivery,[27, 28] being an aqueous process that relies on the alternating adsorption of material species through complementary interactions.[29] This method has been used to coat a wide range of materials with complex geometries including bone implants and scaffolds,[30] bandages[31] and microneedles,[32, 33] made of a diverse array of materials such as stainless steel, titanium or polystyrene. The LbL technique allows for high material incorporation (10–40 wt.%) of sensitive therapeutic

compounds (e.g. cytokines, RNA, or DNA) with nanoscale precision, a striking advantage in comparison with other strategies such as polymer blending,[34] often used to produce functional electrospun fibers.

In the context of soft tissue wound care, our approach offers the potential for a number of unique benefits by combining these methods. Taking a cue from how nature facilitates interaction with soft tissues, namely using prominent protrusions (e.g. spiny-backed orb-weavers, *Gasteracantha cancriformis*), we create for the first time electrospun constructs with enhanced 3D microprotrusions (Fig. 1). Such structures are beneficial for wound care, since they are characterized by having higher friction factors and Nusselt numbers,[35] which improve mechanical interlocking with soft tissues, heat dissipation and increased contact with the wound. Moreover, the unique reported manufacturing process allows to generate dressings that are impermeable to external liquid-form sources of infection (e.g. sweat), while keeping an inner structure suitable to wound exudate uptake and balanced moisture retention. The generated scaffolds are still characterized by the traditional high porosity and tortuosity of two-dimensional electrospun constructs, a key aspect to allow the required gaseous exchange during the wound healing process. Functionalizing these biologically inspired 3DECs with LbL films provides a means to modulate surface-tissue interaction, avoiding cellular adhesion on the dressings and therefore contributing for the dressing's painless removal, while continuously releasing active agents for the wounded tissue regeneration, as well as it allows to alter the transport and physical characteristics of the electrospun scaffolds. In this work, we describe the combination of cutting-edge electrospinning techniques and LbL functionalization to generate biologically inspired three-dimensional multilayered electrospun constructs, a methodology that can be used to enhance potential two-dimensional fibrous materials[36–38] or current production methodologies[39–43] with no further complexity.

Experimental Section

Fabrication of three-dimensional multilayered electrospun constructs

Poly(ε-caprolactone) (PCL, Mw ~ 65.0×10^3 g.mol^{-1}, Sigma-Aldrich) was dissolved in a 40/60 (v/v) solution of acetic (99.8%, Riedel-de Haën) and formic acid (≥98%, Sigma-Aldrich) at a desired concentration of 35 wt.%. The polymer solution was magnetically stirred for 4 h at room temperature and, posteriorly its shear viscosity was measured at 25 °C in a shear range of 1–10^3 s^{-1} by using a rotational rheometer (Gemini HR nano). The PCL polymer solution was pumped through a metallic capillary (21 gauge) by using a syringe pump (Nexus 6000, Chemyx) with a flow rate of 1.0 mL.h^{-1} during 4 hours. The metallic capillary was positively charged by a DC power supplier (Alpha Series II, Brandenburg) at 28 kV, and a 25×25 cm ground aluminum foil was vertically displaced at a tip-to-collector distance of 16 cm. Both the capillary and collector were within a glass sealed box with a controlled surrounding temperature (31.0 ± 0.1 °C). The glass sealed box also comprised a ventilation system to control the relative humidity level (30.0 ± 1.0 %) and solvent content in the working atmosphere. For plasma modification, the scaffolds were placed on a nonporous metallic plate, holding their edges with a glass frame and placed inside a 2 dm^3 radio frequency tubular reactor (Plasma System Fento v5.0, Diener). After chamber

evacuation, argon was supplied into the working environment during 5 minutes prior to the treatment. The pressure within the chamber was kept at 0.4 mbar and a power intensity of 80 W was applied during 5 and 10 minutes. Posteriorly, the electrospun constructs were exposed to air. In order to produce three-dimensional multilayered electrospun constructs (3DMECs), samples were plasma cleaned for 30 seconds and soaked in a 10 mM linear polyethyleneimine (LPEI, Mw ~ 25.0×10^3 g.mol^{-1}, Polyscience Inc.) solution for 30 minutes. Excessive media was posteriorly removed by vacuum filtration before spray-LbL. The electrospun materials were fixed in a metallic grid displaying their top side towards the nozzles. Films were prepared using a programmable spray LbL apparatus (Svaya Nanotechnologies), in a similar fashion as reported in literature.[44, 45] Briefly, polyelectrolytes were alternately sprayed during 20 seconds with an intermediary wash step of 5 seconds. Chitosan (CHI, Mw ~ 15.0×10^3 g.mol-1, Polyscience Inc.) with a reported[46] was used as polycation, while hyaluronic acid (HA, Mw ~ 2.0×10^6 g.mol^{-1}, Lifecore Biomedical) with a reported[47] pKa ~ 2.9 was used as polyanion. Prior to bilayer deposition, LPEI and dextran sulfate (DS, Mw > 500.0×10^3 g.mol^{-1}, Sigma-Aldrich) were initially sprayed in order to promote the formation of a $(LPEI/DS)_{10}$ baselayer.

Constructs morphology characterization

3DECs and 3DMECs were coated with a 10 nm layer of Au/Pd and observed by Scanning Electron Microscopy (JSM-6010LA, JEOL). The observed topographical features were computationally segmented by using ImageJ (NIH). As-spun 3DECs porosity and pore size distribution was determined by mercury porosimetry (Autopore IV porosimeter, Micromeritrics) as described in the literature.[48] The mercury surface tension and its intrinsic contact angle with the electrospun constructs was considered to be γ_{Hg}=480 mN.m^{-1} and θ=140°. In order to cross-validate the porosity value obtained through the mercury porosimetry data, Equation 1 was used:

$$\text{Porosity}\,(\%) = 100 * \left(1 - \frac{m_{3DEC}}{V_{3DEC}} * \frac{1}{\rho_{PCL}}\right), \text{ with } \rho_{PCL} = 1.145\ \text{g.cm}^{-3} \quad (1)$$

Constructs chemical characterization

The scaffolds bulk chemical characterization was studied by proton nuclear magnetic resonance (^{1}H-NMR, ARX 400 MHz, Bruker) and Fourier Transform Infrared Spectroscopy (FTIR, Spectrum 1000, Perkin Elmer). The constructs surface chemical composition was studied by X-ray Photoelectron Spectroscopy (XPS, XSAM800, Kratos Analytical) and static contact angles (CAM 100, KSV Goniometer). Technical details about sample preparation and analysis are explained in the supplementary information.

In vitro swelling ratio

Rectangular samples (2×1 cm^2) of each type of the three-dimensional dressing were initially weighted (W_0) and then incubated in Acetate Buffer Solution (ABS, pH=5.0 0.1 M), Phosphate Buffer Solution (PBS, pH=7.4 0.1 M) and TRIS Buffer Solution (TBS, pH=8.0 0.1 M) at room temperature during 30 days (N=4). Each beaker contained 10 mL of medium. Periodically, the samples were removed from the swelling medium and wiped to

remove the excess of buffered medium. After weighing the swelled dressings (Wt), each sample returned to the original beaker. The swelling ratio (SR) was determined by the following equation:

$$SR = \frac{W_t}{W_0} \quad (2)$$

In vitro degradation and mechanical properties

Circular shape specimens (diameter=1cm) of untreated and plasma treated electrospun constructs were incubated in ABS, PBS and TBS media at room temperature during 30 days after being initially weighted (Wm_0). Each beaker contained 1 mL of medium. Periodically, samples were removed from the medium, gently washed with distilled water for five times, lyophilized during 24 hours and then once more weighted (Wm_t), while in parallel the erosion media were stored at −18.0 °C. The degradation process was assessed by the percentage of weight loss (N=4) and UV spectroscopy. The percentage of weight loss (WL) was determined by the following equation:

$$WL\,(\%) = \frac{Wm_t}{Wm_0} * 100 \quad (3)$$

The UV absorbance at 250 nm was measured for each erosion media (Lambda 25, Perkin Elmer), since such wavenumber is attributed to the $n \rightarrow \pi^*$ transition of the ester carbonyl in a PCL polymeric component.[49, 50] The mechanical properties of the electrospun dressings were tested with a tensile testing machine (MINIMAT firm-ware v.3.1) at room temperature. The samples were cut into 2×1 cm^2 strips and immersed in PBS, ABS and TBS medium during 30 days. Periodically, the specimens were removed and their tensile properties were assessed until rupture (N=4). In addition, the mechanical properties of as-spun constructs were also analyzed. The initial length between the clamps was set at 1 cm with a testing speed of 0.2 $mm.min^{-1}$.

Water Vapor Transmission Rate

Specimens (N=4) were initially conditioned for 24 hours in a desiccator (room temperature, 30% relative humidity) to achieve moisture content equilibrium. A glass tube with a 1 cm^2 opening area (A) was filled with 2 mL of distillated water and covered with a circular sample. The glass tube was then placed in a tube flask with a saturated solution of K_2CO_3 in a temperature controlled storage unit (25.0 ± 1.0 °C), re-weighing daily the assembly glass tube + construct (m). WVTR was calculated by the following equation:

$$WVTR\left(g.cm^{-2}.day^{-1}\right) = \frac{\Delta m}{A * time} \quad (4)$$

Thermal Insulation

3DECs and 3DMECs were initially conditioned for 24 hours at room temperature. 3×3 cm^2 samples were place in a 2×2 cm^2 polystyrene frame with a thickness of 5 cm, covering a

$5\times5\times10$ cm^3 heating chamber with a temperature controlled heating plate. The heating environment was set at an equilibrium temperature of 37 °C with a relative humidity of 30–35 %. The chamber temperature was continuously measured by a local thermocouple. The samples were placed in such way that the side with the multiple protrusions was in contact with the heated environment, while the smooth side was facing the external environment (room temperature). A second thermocouple was placed in close contact with this side, allowing the recording of any superficial temperature variation. The experiment was run during 3 hours (N=3).

Film thickness and surface characterization

Glass and silicon substrates were sprayed in a similar fashion as described earlier, being afterwards dried under a gentle nitrogen flow. Prior to film construction, the substrates were sequentially cleaned with methanol, ethanol, 2-propanol and milli–q water. Spray-coated glass slides (N=3) were scored by a razor blade and the step height difference, between untouched film regions and the score's bottom was tracked at nine different locations by profilometry (Dektak 150, Veeco). In addition, a $(CHI/HA)_{10}$ 30×30 μm^2 film area was examined by Atomic Force Microscopy (Dimension 3100 AFM, Veeco Metrology) in tapping mode.

Hyaluronic acid release studies

HA fluorescence dye was synthesized for confocal microscopy use and release studies, and its synthesis process is detailed in the supplementary information. The HA release profile of the produced 3DMECs at 37 °C was determined in two different media: PBS (pH=7.4 0.1 M) and cell conditioned media. Cell conditioned media was prepared from NIH-3T3 cells grown to confluence. An initial cell concentration of 50×10^3 was seeded into a 24-well plate and cultured in Advanced-MEM (Invitrogen) media containing 5% FBS, 1% antibiotic-antimitotic and 2mM L-glutamine. After 72 hours, media was removed and filtered with a 0.2 μm syringe filter in order to remove cellular debris. Posteriorly, circular specimens (diameter=1cm) were incubated in 1.5 mL of each media (N=3). At a given interval, 250 μL of medium was replaced. A standard curve of the FITC-HA was used to interpret the concentration of HA in the release media (excitation peak = 492 nm).

Scratch assay

The scratch assay, an *in vitro* technique consisting on the formation of an artificial scratch in a confluent cell monolayer,[51–53] is used to evaluate the rate of wound closure promoted by the generated LbL coated fibrous materials. Briefly, NIH-3T3 (GFP+) cells, with an initial concentration of 20×10^3, were seeded into a 24-well plate and grown to a sub-confluent (80–90%) monolayer. The resultant monolayer was then wounded with a sterile 200 μL pipette tip. The gap consisted in a straight line scratch across each well, being posteriorly washed with PBS (pH=7.4 0.1 M) in order to remove cellular debris and culture further with media containing degraded polymer material. Uncoated (A-type 3DECs) and coated 3DEMCs ($A+(CHI/HA)_{10}$ and $A10+(CHI/HA)_{10}$) were incubated at 37 °C in PBS (pH=7.4 0.1 M) during 7 days. At the end of the incubation period, the media with soluble degraded polymer products was filtered with a 0.2 μm syringe filter and diluted (50% v/v) in fresh

Advanced-MEM (Invitrogen) media containing 5% FBS, 1% antibiotic-antimitotic and 2mM L-glutamine. Each final formulation was applied to the wounded cell monolayer (N=4). Scratch width was followed during a 48 h period (Axiovert 200, Zeiss), in which the scratch width was determined by the gap from opposing wound edges, while considering four measurements per field of view. The wound closure was then expressed as a percentage of the initial wound gap.

Results and Discussion

Production and morphological characterization of three-dimensional electrospun constructs (3DECs)

Poly(ε-caprolactone), a biocompatible aliphatic polyester, was used to manufacture 3DECs for wound healing applications. In addition to its long-term degradation in physiological media,[54] PCL presents several advantages over other polymers that meet the specifications for an ideal wound dressing (Table S1). It has been demonstrated that PCL could be polarized under intense electric fields by controlling the surrounding relative humidity, favoring the formation of 3DECs.[22] Nevertheless, thus far PCL had been assembled only into microfibrous constructs that generate honeycomb patterns,[22, 55] a type of topography with limited applications. In this work, we generated 3DECs with multiple protrusions on the top surface, while maintaining a flat bottom surface (Fig. 2A, B and C).

The bottom side, which corresponds to the side in contact with the grounded collector, is characterized by a random fiber deposition, commonly observed as well in 2DECs.[44, 56, 57] On this side, the scaffolds exhibited a bimodal fiber diameter distribution: Population 1, fiber diameter = (21 ± 9)×10 nm; Population 2, fiber diameter = (15 ± 4)×10^2 nm (Fig. S1). We hypothesize that the bimodal distribution is related to the instability of the electrospun polymer jet due to the intense electric field, a phenomenon also reported in the production of 2DECs.[58] The top side of the construct shows multiple conical protrusions, resulting from the preferential deposition of fibers in specific regions driven by local *in situ* polarization of high dense fiber regions in the plane of the collector.[22] The electrostatic attraction between these regions and the depositing fibers promotes the localized preferred deposition of fibers and the generation of sub-millimeter features over time (Fig. S2). The generated 3DECs demonstrated a median protrusion density of 73 peaks.cm^{-2}, while the median inter-protrusion distance was 528 μm (Fig. S3). As a consequence of the fibers' preferential deposition, each protrusion shows a z-axis densely packed fibrous core (Fig. 2D, Fig. S4). As determined by mercury porosimetry, the fibrous materials have a multimodal pore size distribution (Fig. 2F), with an overall porosity of 89.9% (92.7% when considering Equation 1) and a surface area of 1.44 $m^2.g^{-1}$, values in the range of what is expected for electrospun materials.[59]

The protrusion geometric characterization was evaluated at two dressing configurations: (i) flat (conformation corresponding to a superficial wound), or (ii) curved (conformation corresponding to a full thickness wound) (Fig. 2E). After being bent (bend angle = 110 °), the protrusions are effectively reduced in height by 37.6%, while the inter-protrusion distance is increased by 50.7%. 3DECs can thus offer topographical features that support the dressing fixation at the wound bed in a broad range of wounds,[60] a feature lacking in

traditionally used wound dressings. One property of an ideal wound dressing is the capability to be impermeable to external liquids so as to avoid sources of infection, while allowing the uptake of wound exudate. For our bandage to achieve this property, we proposed to treat differentially each side of the construct in order to create a hydrophilic gradient across the bandage, in association with the already generated z-axis construct asymmetry. Therefore, to reduce the PCL-based 3DECs hydrophobicity, the materials were plasma treated in argon and then exposed to atmospheric air. We chose to use an inert gas to avoid the 3DECs surface ablation or etching, otherwise observed with reactive gases such as oxygen.[61] To determine the effect of this treatment, three groups of 3DECs were investigated: A, 3DECs without plasma treatment; A5, 3DECs plasma treated for 5 min, and A10, 3DECs plasma treated for 10 min. After solubilizing as-spun 3DECs in $CDCl_3$, ^{1}H-NMR spectra were acquired (Fig. S5), indicating the complete absence of the acetic and formic acid initially used to prepare the PCL. Contact angle measurements of both top and bottom sides of each construct validated our approach, as the bottom untreated side was unchanged from the control, while the plasma treated groups exhibited a significantly lower contact angle on their top surface than the untreated control (Fig. S6A). The plasma treatment creates a hydrophilic gradient across the materials, in which their top sides are the most hydrophilic regions of the dressings. 3DECs were delaminated and portions from the top and bottom of the construct were analyzed by FTIR and XPS (Fig. S6B–D), showing stronger ν(OH), ν(C=O) and ν(C–O) signals in comparison with the non-treated ones.

Moreover, it was possible to observe on the plasma treated constructs, a noticeable difference of these signals between their top and bottom sides. In addition, XPS characterization demonstrated a higher O/C ratio in the plasma treated samples, supporting the preferential development of oxygenated hydrophilic groups (-OH, -COOH) near the top surface of the constructs.

Fluid uptake directionality and long-term mechanical stability

Prior to studying the fluid uptake directionality, the 3DECs mechanical properties were determined, showing no significant change after using plasma treatment to modify the materials top side (Fig. 3A). 3DECs evidenced an initial non-linear stress-strain response (toe region), followed by a stiff linear region characteristic of an elastic domain, which we hypothesize is due to the alignment of the randomly oriented fibers as often observed in 2DECs.[62]

These self-assembled materials are highly elastic compared with recently produced PCL-based 2DECs (E, Elastic modulus: E_{2DECs}=19 ± 2 MPa), while maintaining a relatively high ultimate tensile strength (UTS) despite having a lower value (UTS_{2DECs}=2.50 ± 0.08 MPa).[63] However, it is important to notice that even the lowest UTS value observed (UTS_{A10}=1.9 ± 0.1 MPa) corresponds to apply (19 ± 1)×10^4 kg in 1 m^2 of the dressing area, an unlikely situation to occur when a patient is using a wound dressing. Despite the elastic modulus of human skin ranging between 4.5 to 8 kPa,[64] it has been demonstrated that the proliferation rate of human dermal fibroblasts is directly proportional to the stiffness of their tested substrates (E=0.5–120 MPa).[65] In this way, it is expected that 3DECs are capable to enhance cellular proliferation while being mechanically suitable to fit non-uniform wound

sites. Another characteristic of an ideal wound dressing is the reduction of the necessary is the reduction of the necessary dressing changes,[66, 67] which is usually limited by the dressing physicochemical properties and mechanical stability. To evaluate whether 3DECs could be easily replaced, we investigated the dressing properties in three different simulated wound exudate pH conditions for up to 30 days. Plasma treated 3DECs showed an increased weight loss compared with the untreated controls, however the overall degradation was less than 3 wt% (Fig. 3C). These findings were cross-validated with UV absorbance measurements at 250 nm, corresponding to the n→π* transition of the ester carbonyl in PCL (Fig. 3D). The swelling ratio of the surface modified and unmodified constructs was also assessed over the 30-day study period. The plasma treated 3DECs also demonstrated a higher swelling ratio compared to untreated materials, improving their capability to absorb wound exudate (Fig. 3B). In comparison with the chemically unmodified scaffolds, and regardless of the medium pH, A5 and A10 exhibited a continuous swelling decay after day 4. Since we previously confirmed a degradation lower than 3 wt% for these materials, we hypothesize that this decay results exclusively from the progressive re-organization of the bottom fibrous network after the maximum swelling ratio has been reached. The absorption process consists in a fluid entering in a scaffold by diffusion and being drawn by capillary force into the porous regions.[68] The continuous water uptake leads to the adherence of a water layer on the fiber surface, which reduces the fiber-fiber drag force under stress. In this way, at the maximum swelling ratio, the generated inner pressure promotes fibrous network re-orientation due to fiber-fiber sliding, resulting in a smaller average pore size and consequent expelling of fluid. Fiber hydration is likely responsible for the reduction of the 3DEC elastic modulus and UTS (Fig. 3E), which is a common phenomenon found in the traditional 2DECs when wetted.[69, 70] Nonetheless, at day 14 and a pH=7.4, A, A5 and A10 constructs still have the ability to absorb $(12.7 \pm 0.6)\times10^4$ kg, $(11.3 \pm 0.2)\times10^4$ kg and $(11.0 \pm 0.3)\times10^4$ kg of water per m^2 of dressing area respectively, where the typical dressing thickness is 3.7 ± 0.1 mm, while demonstrating the mechanical properties needed for dressing changes when necessary.

Characterization of uptake and directionality of a liquid, according to each side of the 3DECs, was done by investigating both liquid spreading on the dressing surface and imbibition into the dressing inner structure. As shown in Fig. 2, the induced z-axis asymmetric fiber deposition in 3DECs favors the formation of a protective fibrous bottom layer due to a higher fiber density in this side. Therefore, the produced 3DECs have a pore size and hydrophobic gradient across the scaffolds' thickness that favors fluid handling properties. Analogous to Martins et al.,[71] we chose to use glycerol for the contact angle measurements due to the similarity of its surface tension ($\gamma_{25°C}$=62.4 $mN.m^{-1}$) with water surface tension ($\gamma_{25°C}$=72.0 $mN.m^{-1}$) and its viscosity, which is comparable to that of wound exudate. Time-lapse contact angle measurements showed similar droplet behavior on the bottom side of all 3DECs, where droplet spreading and imbibition did not take place (Fig. S7). The first stage of a drop motion in contact with a dressing is the spreading, meaning the motion of the three-phase contact line through the dressing surface (Scheme S1). In the case of the 3DECs bottom side, the differences in the polarity of the non-functionalized PCL fibers and glycerol hindered wetting, which in turn inhibits liquid imbibition. Due to the z-axis asymmetric fiber deposition, the 3DECs topography at the top

side is microtexturized. This, in combination with the higher hydrophilic functionalization, offers a distinct environment for liquid spreading and imbibition. The surface functionalization of the dressings A5 and A10, in comparison with the A type constructs, significantly accelerated spreading by an order of magnitude as well as reduced the total liquid imbibition time to approximately 3 minutes, compared to an approximated 14 minutes in the A type dressings (Fig. 3G). While the bottom side of the 3DECs is structurally and chemically similar, their top sides are only morphologically similar, leading to different spreading and imbibition dynamics. Conversely, comparing the top and bottom sides of the A type wound dressings, which have the same chemical composition, it is possible to observe a distinct drop in spreading and imbibition at the top side. This suggests that the topography of the 3DECs is also important. It is likely due to the increased porosity and subsequent increase in permeability of the construct on its top side, caused by the reduction of resistance of the porous medium to flow. Thus, the observed pore size gradient across the membrane thickness also favors the wound exudate transport from the top side to the bottom side, while simultaneously hindering the imbibition of external contaminated liquids in the opposite direction.

LbL coating and *in vitro* assessment of the modified multilayered electrospuns constructs

With the successful fabrication of 3DECs, possessing desirable mechanical and structural properties for wound dressings, we aimed to incorporate increased functionality to the surface of the bandage through the use of LbL coatings. An ideal bandage surface would both promote wound healing as well as impair tissue integration into the construct.[66] These properties would reduce the time that the bandage would need to be in contact with the wound and reduce the pain associated with bandage changes. Based on their widely reported benefits in wound healing applications we chose to incorporate the combination of chitosan (CHI) and hyaluronic acid (HA).[72, 73] Chitosan is a poly-cationic species and has been used extensively in wound dressings as an anti-microbial and pro-clotting agent.[74] Hyaluronic acid is also widely used in bandages and resorbable matrices due to its high biocompatibility and role in the natural extracellular matrix.[75] To reduce tissue integration into the dressing we aimed to achieve a coating that both bridges the pores of the top of the construct, providing a physical barrier to penetration, and has a low elastic modulus to reduce cell adherence.[76] Films were deposited on the plasma treated surface of the 3DECs by the spray-LbL method which was not observed to significantly alter the structure of the 3DECs (Fig. S8–S9). The film architecture of $(CHI/HA)_x$, where x is the number of bilayer repeats, was first studied by assembling films on oxygen plasma treated glass substrates. Thickness and roughness properties of the film were determined by profilometry (Fig. 4A).

The film was observed to deposit in a near-linear fashion with an average growth rate of 25 ± 4 nm per bilayer (R^2=0.98), reaching a thickness of (26 ± 4)×10 nm after 10 bilayers. Coating of 3DECs was performed similarly, generating three-dimensional multilayered electrospun constructs (3DMECs). To evaluate the uniformity of the coating, fluorescently labeled HA was used in film assembly and coated substrates were imaged via fluorescent imaging (Fig. 4B). The 3DMECs were successfully coated by the LbL film while preserving their unique topography. Moreover, by comparing the top and bottom sides of 3DMECs, the materials showed significantly increased material adsorption to their top surface side (Fig.

S10), which is expected due to the direction of film deposition and the constructs' unidirectional permeability.

Confocal microscopy (Fig. 4C) and scanning electron microscopy (Fig. 4D), were also used to assess the LbL coating on the 3DMECs. Both techniques showed a uniform coating of the protrusions and their interspaces. SEM imaging also suggested little to no coating on the bottom side of the scaffolds, with the electrospun fibers appearing similar to uncoated substrates. Despite the film adherence and uniformity of the coating on the construct, there is very little penetration of the film into the porous fibrous network within the material (Fig. S11). The process of spraying also yielded a unique morphology to develop on the surface of the 3DMECs, generating particles with an average diameter of 6 ± 4 μm on the construct surface, primarily in the interspaces between protrusions (Fig. S12). We hypothesize that the poor film interpenetration as well as the particle generation were related to both the pressure gradient across the materials and the HA solution viscosity. Due to the hygroscopic nature of chitosan and hyaluronic acid, water uptake contributes to the generation of a rubbery film layer,[77] with poor rigidity and consequent reduced cellular adhesion on the top of the scaffold (Fig. S13). In contrast, when NIH-3T3 cells were purposely seeded in the 3DMECs lacking the LbL film coating, there was significant cellular adhesion (Fig. S14).

To determine the effect of the film coating on important wound dressing properties, we evaluated the changes in swelling ratio, water vapor transmission, and thermal insulation for coated and uncoated constructs. The LbL film coatings led to significant increases in the swelling of the dressings (Fig. 5A), achieving a 1.6-fold increase in the A10 type constructs over its uncoated control. The combination of the plasma treatment and LbL functionalization, allows the generation of a range of wound dressings with different absorption capabilities, a versatile feature for physicians selecting the proper wound dressing for a patient.[78]

As important as the ability to promote the uptake of wound exudate, the water vapor transmission rate (WVTR) is critical when selecting a wound dressing. Ideal dressings must favor the presence of a moist wound environment to avoid dehydration and dressing adherence, while avoiding maceration of the healthy surrounding tissue.[79] Non-plasma treated three-dimensional electrospun wound dressings consistently demonstrated increased WVTR compared to commercially available dressings (Fig. 5B), which is primarily due to the 3DECs porosity and thickness. Incorporation of LbL in 3DECs caused a significant drop in WVTR, which we hypothesize is due to increased water retention within the $(CHI/HA)_{10}$ film due to swelling and the film's role as a barrier to diffusion. The thermal insulation of a recovering wound has also been highlighted as an important feature in the design of wound dressings which can significantly impact wound healing.[80–82] When wound-tissue temperature falls below 33 °C neutrophil, fibroblast and epithelial cell activity decreases,[83] leading to a poor healing. In our assessment (Fig. 5C), both 3DECs and 3DMECs have shown the ability to thermally insulate a wound bed environment.

After demonstrating that the $(CHI/HA)_{10}$ film coating can significantly reduce cell adhesion to the coated bandage while maintaining its desired properties as a wound dressing, we set out to determine if the incorporated materials, in particular HA, had an *in vitro* healing

benefit. Hyaluronic acid has been reported to interact with cell surface receptors as CD44, RHAMM and ICAM-1, favoring cellular proliferation and migration.[84] The release of fluorescent labeled HA from hydrated bandages was evaluated in PBS and in cell conditioned media at 37 °C for 7 days (Fig. 6A). Release of HA from 3DMECs was sustained for the seven day period with a linear profile regardless of the type of construct or release media. A-type 3DECs were observed to release more HA during the study period in both environments, releasing nearly all of the coated HA in cell conditioned media (Fig. 6B). A10-type dressings showed the slowest and most sustained HA release comparatively to the other specimens. Due to their distinct HA incorporation and release profiles, uncoated, A-type, and A10-type three dimensional scaffolds were used for *in vitro* scratch assays.

In general, groups treated with release media from 3DECs coated with $(CHI/HA)_{10}$ were observed to close the scratch faster than uncoated control bandage treated groups (Fig. 6C, D). After 48 hours, A-type and A10-type 3DMECs reached 87 ± 4 % and 90 ± 0.5 % of wound closure respectively, in contrast to 70 ± 2 % observed in groups treated with the uncoated 3DECs. Cell shape was assessed within the scratch region to help determine the cellular behavior and proliferation within the defect. Groups treated with 3DMECs showed significantly reduced cell areas and increased cell circularity compared to uncoated controls after only 12 hours and was sustained for the two day test period. This supports the hypothesis that the released material promotes cell proliferation, suggesting that confluence is reached sooner when using these LbL coated constructs.

Conclusion

In this work we produced for the first time three-dimensional multilayered electrospun constructs. The generated scaffolds are characterized by a flat bottom side and a top side populated with fibrous-based microsized protrusions, which have a median inter-protusion distance of 528 μm and a median peak density of 73 peaks per cm^2. These constructs can be readily produced by taking advantage of the self-organization phenomena when electrospinning PCL nanofibers. As prepared these materials are capable of withstanding $(11.0 \pm 0.3)\times10^4$ kg per m^2 after 14 days of hydration. Their unique asymmetry promotes unidirectional liquid uptake (from the top side towards the inner structure of the materials), while being impermeable to potential external liquid-forms of infection at its bottom side. Nevertheless, such constructs also observed the high porosity (89.9%) and high surface area ($1.44\ m^2.g^{-1}$) characteristic of traditional electrospun mats. To incorporate broader functionality into these dressings we used spray-LbL assembly to create an ultrathin coating on the top surface of the scaffolds consisting in chitosan and hyaluronic acid, two biocompatible polymers widely used in the field of wound care. This coating reduced cellular adhesion on the constructs throughout the generation of a rubbery film layer, which would also provide a means to tailor water vapor transmission and swelling ratio for different wound environments specifications (e.g. ischemic wounds, I/II/III-degree burns, etc.). Moreover, the three-dimensional fibrous constructs treated with LbL were able to achieve 90 ± 0.5 % of wound closure within 48 hours, comparatively to 70 ± 2 % verified for uncoated dressings. This work provides an important first step in producing electrospun wound dressings that can better meet the needs of medical practitioners and improve patient

care, while taking advantages of already two-dimensional fibrous bandages and fabrication methods.

Supplementary Material

Refer to Web version on PubMed Central for supplementary material.

Acknowledgments

We thank the Financial support from Fundação Calouste Gulbenkian, Fundação para a Ciência e a Tecnologia (FC&T), through the contracts UID/QUI/50006/2013, MIT-Pt/BS-CTRM/0051/2008, PTDC/EMETME/103375/2008, the doctoral grant SFRH/BD/51188/2010 (TCR), MIT-Portugal Program (Bioengineering Systems Focus Area) FEDER and FSE. This research was also supported in part by funding and core facilities provided by the U.S. Army Research Office under contract W911NF-07-D-0004 at the MIT Institute of Soldier Nanotechnology and by funding from the Sanofi-Aventis and MIT Center for Biomedical Innovation. This work was also supported by use of core facilities at the Koch Institute for Integrative Cancer Research (supported by the NCI under grant 2P30CA014051-39). We thank the Koch Institute Swanson Biotechnology Center for technical support, specifically the microscopy, flow cytometry, and histology cores.

References

1. Wu SZ, Wu D, Yao J, Chen QD, Wang JN, Niu LG, Fang HH, Sun HB. Langmuir. 2010; 26:12012. [PubMed: 20499864]
2. Li Y, Zhang J, Yang B. Nano Today. 2010; 5:117.
3. Downing TL, Soto J, Morez C, Houssin T, Fritz A, Yuan F, Chu J, Patel S, Schaffer DV, Li S. Nat Mater. 2013; 12:1154. [PubMed: 24141451]
4. Viswanathan P, Ondeck MG, Chirasatitsin S, Ngamkham K, Reilly GC, Engler AJ, Battaglia G. Biomaterials. 2015; 52:140. [PubMed: 25818420]
5. Yin Z, Chen X, Song H-x, Hu J-j, Tang Q-m, Zhu T, Shen W-l, Chen J-l, Liu H, Ouyang BC, Heng H-W. Biomaterials. 2015; 44:173. [PubMed: 25617136]
6. Morgado PI, Aguiar-Ricardo A, Correia IJ. J Membr Sci. 2015; 490:139.
7. Morgado PI, Lisboa PF, Ribeiro MP, Miguel SP, Simões PC, Correia IJ, Aguiar-Ricardo A. J Membr Sci. 2014; 469:262.
8. Wegst UG, Bai H, Saiz E, Tomsia AP, Ritchie RO. Nat Mater. 2015; 14:23. [PubMed: 25344782]
9. Rees A, Powell LC, Chinga-Carrasco G, Gethin DT, Syverud K, Hill KE, Thomas DW. Biomed Res Int. 2015; 2015:925757. [PubMed: 26090461]
10. Bhardwaj N, Kundu SC. Biotechnol Adv. 2010; 28:325. [PubMed: 20100560]
11. Agarwal S, Greiner A, Wendorff JH. Prog Polym Sci. 2013; 38:963.
12. Zhou X, Dai Z, Liu S, Bao J, Guo YG. Adv Mater. 2014; 26:3943. [PubMed: 24664966]
13. Persano L, Camposeo A, Tekmen C, Pisignano D. Macromol Mater Eng. 2013; 298:504.
14. Lee BLP, Jeon H, Wang A, Yan Z, Yu J, Grigoropoulos C, Li S. Acta Biomater. 2012; 8:2648. [PubMed: 22522128]
15. Jenness NJ, Wu Y, Clark RL. Mater Lett. 2012; 66:360.
16. Sun B, Long YZ, Zhang HD, Li MM, Duvail JL, Jiang XY, Yin HL. Prog Polym Sci. 2014; 39:862.
17. Bonino CA, Efimenko K, Jeong SI, Krebs MD, Alsberg E, Khan SA. Small. 2012; 8:1928. [PubMed: 22461238]
18. Sun B, Long YZ, Yu F, Li MM, Zhang HD, Li WJ, Xu TX. Nanoscale. 2012; 4:2134. [PubMed: 22344309]
19. Liang T, Mahalingam S, Edirisinghe M. Mater Sci Eng, C. 2013; 33:4384.
20. Nedjari S, Schlatter G, Hébraud A. Mater Lett. 2015; 142:180.
21. Okuzaki H, Takahashi T, Miyajima N, Suzuki Y, Kuwabara T. Macromolecules. 2006; 39:4276.
22. Reis TC, Correia IJ, Aguiar-Ricardo A. Nanoscale. 2013; 5:7528. [PubMed: 23836136]

23. Sun XY, Shankar R, Börner HG, Ghosh TK, Spontak RJ. Adv Mater. 2007; 19:87.
24. Sionkowska A. Prog Polym Sci. 2011; 36:1254.
25. Huang JC. Adv Polym Tech. 2002; 21:299.
26. Sill TJ, von Recum HA. Biomaterials. 2008; 29:1989. [PubMed: 18281090]
27. Richardson JJ, Björnmalm M, Caruso F. Science. 2015; 348
28. Hammond PT. AlChE J. 2015; 61:1106.
29. Borges J, Mano JF. Chem Rev. 2014; 114:8883. [PubMed: 25138984]
30. Shah NJ, Hyder MN, Moskowitz JS, Quadir MA, Morton SW, Seeherman HJ, Padera RF, Spector M, Hammond PT. Sci Transl Med. 2013; 5:191.
31. Castleberry S, Wang M, Hammond PT. ACS Nano. 2013; 7:5251. [PubMed: 23672676]
32. DeMuth PC, Min Y, Huang B, Kramer JA, Miller AD, Barouch DH, Hammond PT, Irvine DJ. Nat Mater. 2013; 12:367. [PubMed: 23353628]
33. DeMuth PC, Su X, Samuel RE, Hammond PT, Irvine DJ. Adv Mater. 2010; 22:4851. [PubMed: 20859938]
34. Hammond PT. Mater Today. 2012; 15:196.
35. Chen Y, Chew YT, Khoo BC. Int J Heat Mass Transfer. 2013; 66:177.
36. Sofokleous P, Stride E, Edirisinghe M. Pharm Res. 2013; 30:1926. [PubMed: 23615857]
37. Lowe A, Bills J, Verma R, Lavery L, Davis K, Balkus KJ Jr. Acta Biomater. 2015; 13:121. [PubMed: 25463501]
38. Huang R, Li W, Lv X, Lei Z, Bian Y, Deng H, Wang H, Li J, Li X. Biomaterials. 2015; 53:58. [PubMed: 25890707]
39. Sofokleous P, Stride E, Bonfield W, Edirisinghe M. Mater Sci Eng C Mater Biol Appl. 2013; 33:213. [PubMed: 25428065]
40. Wade RJ, Burdick JA. Nano Today. 2014; 9:722.
41. Wang X, Ding B, Sun G, Wang M, Yu J. Prog Mater Sci. 2013; 58:1173.
42. Zhang S, Karaca BT, VanOosten SK, Yuca E, Mahalingam S, Edirisinghe M, Tamerler C. Macromol Rapid Commun. 2015; 36:1322. [PubMed: 26033345]
43. Mahalingam S, Edirisinghe M. Macromol Rapid Commun. 2013; 34:1134. [PubMed: 23749758]
44. Krogman KC, Lowery JL, Zacharia NS, Rutledge GC, Hammond PT. Nat Mater. 2009; 8:512. [PubMed: 19377464]
45. Shukla A, Fang JC, Puranam S, Jensen FR, Hammond PT. Adv Mater. 2012; 24:492. [PubMed: 22223363]
46. Liu W, Sun S, Cao Z, Zhang X, Yao K, Lu WW, Luk KDK. Biomaterials. 2005; 26:2705. [PubMed: 15585274]
47. Lapčík L, Lapčík L, De Smedt S, Demeester J, Chabreček P. Chem Rev. 1998; 98:2663. [PubMed: 11848975]
48. Lowery JL, Datta N, Rutledge GC. Biomaterials. 2010; 31:491. [PubMed: 19822363]
49. Muñoz-Bonilla A, Cerrada M, Fernández-García M, Kubacka A, Ferrer M, Fernández-García M. Int J Mol Sci. 2013; 14:9249. [PubMed: 23629663]
50. Christensen PA, Egerton TA, Martins-Franchetti SM, Jin C, White JR. Polym Degrad Stab. 2008; 93:305.
51. Kulkarni M, O'Loughlin A, Vazquez R, Mashayekhi K, Rooney P, Greiser U, O'Toole E, O'Brien T, Malagon MM, Pandit A. Biomaterials. 2014; 35:2001. [PubMed: 24331702]
52. Liang CC, Park AY, Guan JL. Nat Protoc. 2007; 2:329. [PubMed: 17406593]
53. Kramer N, Walzl A, Unger C, Rosner M, Krupitza G, Hengstschläger M, Dolznig H. Mutat Res, Rev Mutat Res. 2013; 752:10.
54. Woodruff MA, Hutmacher DW. Prog Polym Sci. 2010; 35:1217.
55. Ahirwal D, Hebraud A, Kadar R, Wilhelm M, Schlatter G. Soft Matter. 2013; 9:3164.
56. Grafahrend D, Heffels KH, Beer MV, Gasteier P, Möller M, Boehm G, Dalton PD, Groll J. Nat Mater. 2011; 10:67. [PubMed: 21151163]

57. Grey CP, Newton ST, Bowlin GL, Haas TW, Simpson DG. Biomaterials. 2013; 34:4993. [PubMed: 23602367]
58. Hohman MM, Shin M, Rutledge G, Brenner MP. Phys Fluids. 2001; 13:2221.
59. Greiner A, Wendorff JH. Angew Chem Int Ed. 2007; 46:5670.
60. Yang SY, O'Cearbhaill ED, Sisk GC, Park KM, Cho WK, Villiger M, Bouma BE, Pomahac B, Karp JM. Nat Commun. 2013; 4:1702. [PubMed: 23591869]
61. France RM, Short RD. Langmuir. 1998; 14:4827.
62. Neel EAA, Cheema U, Knowles JC, Brown RA, Nazhat SN. Soft Matter. 2006; 2:986.
63. Jin G, Prabhakaran MP, Kai D, Annamalai SK, Arunachalam KD, Ramakrishna S. Biomaterials. 2013; 34:724. [PubMed: 23111334]
64. Pailler-Mattei C, Bec S, Zahouani H. Med Eng Phys. 2008; 30:599. [PubMed: 17869160]
65. Hopp I, Michelmore A, Smith LE, Robinson DE, Bachhuka A, Mierczynska A, Vasilev K. Biomaterials. 2013; 34:5070. [PubMed: 23587444]
66. Ovington LG. Clinics in Dermatology. 2007; 25:33. [PubMed: 17276199]
67. Rieger KA, Birch NP, Schiffman JD. J Mater Chem B. 2013; 1:4531.
68. Markicevic B, Hoff K, Li H, Zand AR, Navaz HK. Int J Multiphase Flow. 2012; 39:193.
69. Kharaziha M, Nikkhah M, Shin SR, Annabi N, Masoumi N, Gaharwar AK, Camci-Unal G, Khademhosseini A. Biomaterials. 2013; 34:6355. [PubMed: 23747008]
70. McManus MC, Boland ED, Koo HP, Barnes CP, Pawlowski KJ, Wnek GE, Simpson DG, Bowlin GL. Acta Biomater. 2006; 2:19. [PubMed: 16701855]
71. Martins A, Pinho ED, Faria S, Pashkuleva I, Marques AP, Reis RL, Neves NM. Small. 2009; 5:1195. [PubMed: 19242938]
72. Price RD, Myers S, Leigh IM, Navsaria HA. Am J Clin Dermatol. 2005; 6:393. [PubMed: 16343027]
73. Ueno H, Mori T, Fujinaga T. Adv Drug Delivery Rev. 2001; 52:105.
74. Anitha A, Sowmya S, Kumar PTS, Deepthi S, Chennazhi KP, Ehrlich H, Tsurkan M, Jayakumar R. Prog Polym Sci. 2014; 39:1644.
75. Collins MN, Birkinshaw C. Carbohydr Polym. 2013; 92:1262. [PubMed: 23399155]
76. Zeng X, Li S. J Mech Behav Biomed Mater. 2011; 4:180. [PubMed: 21262496]
77. Miller-Chou BA, Koenig JL. Prog Polym Sci. 2003; 28:1223.
78. Sussman, C. Wound care: a collaborative practice manual for physical therapists and nurses. Lippincott Williams & Wilkins; USA: 2007.
79. Wu P, Fisher AC, Foo PP, Queen D, Gaylor JDS. Biomaterials. 1995; 16:171. [PubMed: 7748992]
80. Kloth LC, Berman JE, Dumit-Minkel S, Sutton CH, Papanek PE, Wurzel J. Adv Skin Wound Care. 2000; 13:69. [PubMed: 11074989]
81. Whitney JD, Salvadalena G, Higa L, Mich M. J Wound Ostomy and Continence Nursing. 2001; 28:244.
82. McCulloch J, Knight CA. Ostomy Wound Manage. 2002; 48:38. [PubMed: 11968894]
83. McGuiness W, Vella E, Harrison D. J Wound Care. 2004; 13:383. [PubMed: 15517749]
84. Collins MN, Birkinshaw C. Carbohydr Polym. 2013; 92:1262. [PubMed: 23399155]

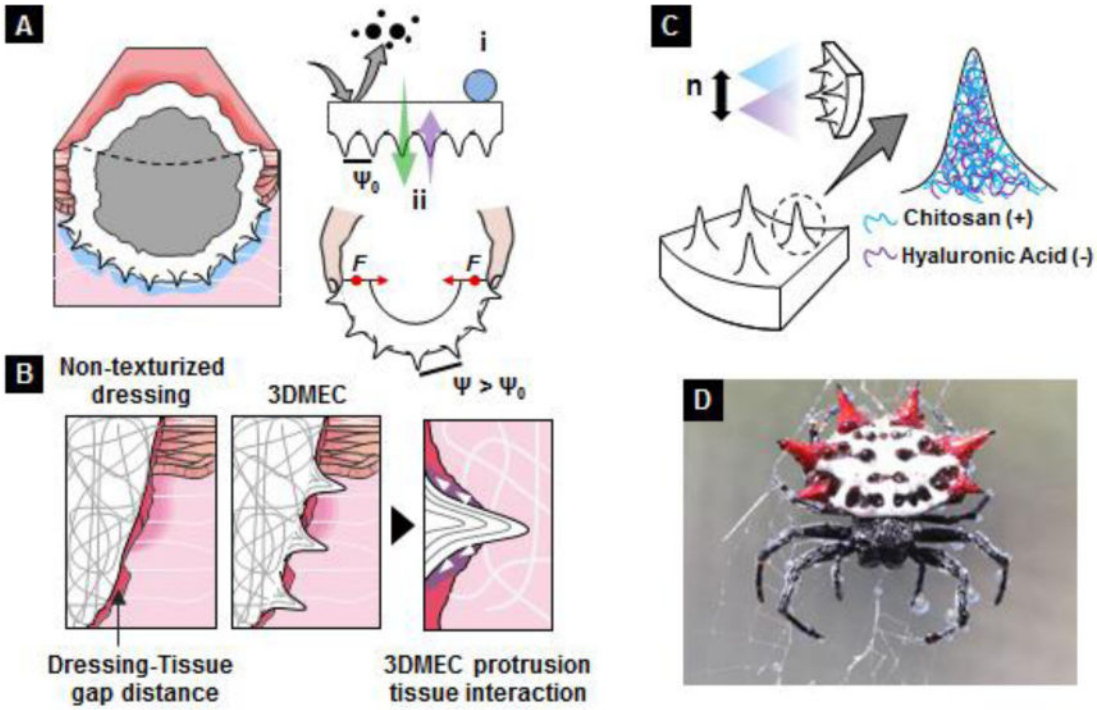

Fig. 1.

Conceptualization of three-dimensional multilayered electrospun constructs (3DMECs). **A**, Concept application as a wound dressing displaying the ideal dressing properties: *i*, impermeability to external infectious microorganisms and liquids; *ii*, gas exchanges across bandage (Ψ, interprotrusion distance). **B**, 3DMEC-tissue interaction in irregular wound bed sites in comparison with traditional dressings. **C**, Chitosan and hyaluronic acid incorporation through spray-LbL. **D**, Photograph of a spiny-backed orb weaver (s.p. Gasteracantha cancriformis) showing prominent protrusions in its abdomen.

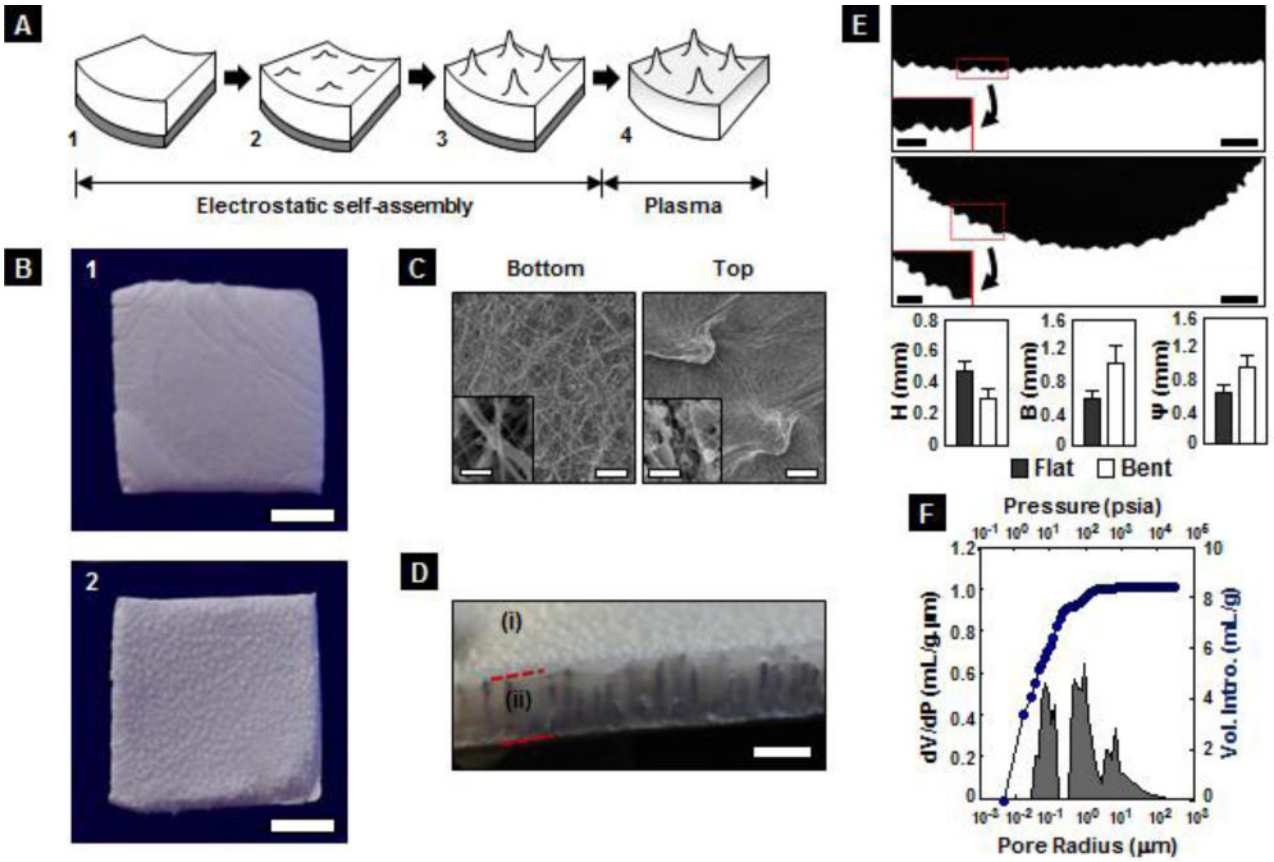

Fig. 2.

Production of 3DMECs. **A**, Scheme of the electrical-driven self-organized 3DECs fabrication process and bottom plasma treatment to improve surface hydrophilicity. **B**, Photograph of the (1) bottom and (2) top side of a 3DEC (scale bar = 1 cm). The top side presents multiple protrusions along the surface with a median protrusion density of 73 peaks.cm^{-2}. **C**, SEM images from bottom and top sides having a scale bar = 100 μm with an inset scale bar = 5 μm. **D**, Photograph of a 3DEC evidencing multiple protrusions at the top side (i) and their z-axis formation in the cross section (ii). Scale-bar = 3 mm. **E**, Micrographs in flat and bent conformations (scale bar = 3 mm, inset scale bar = 1.5 mm) and parametric shape comparison (H, protrusion height; B, equivalent base; Ψ, interprotrusion distance). Data evidence p-value < 0.01. **F**, Mercury porosimetry data after buckling correction for the electrospun materials.[45]

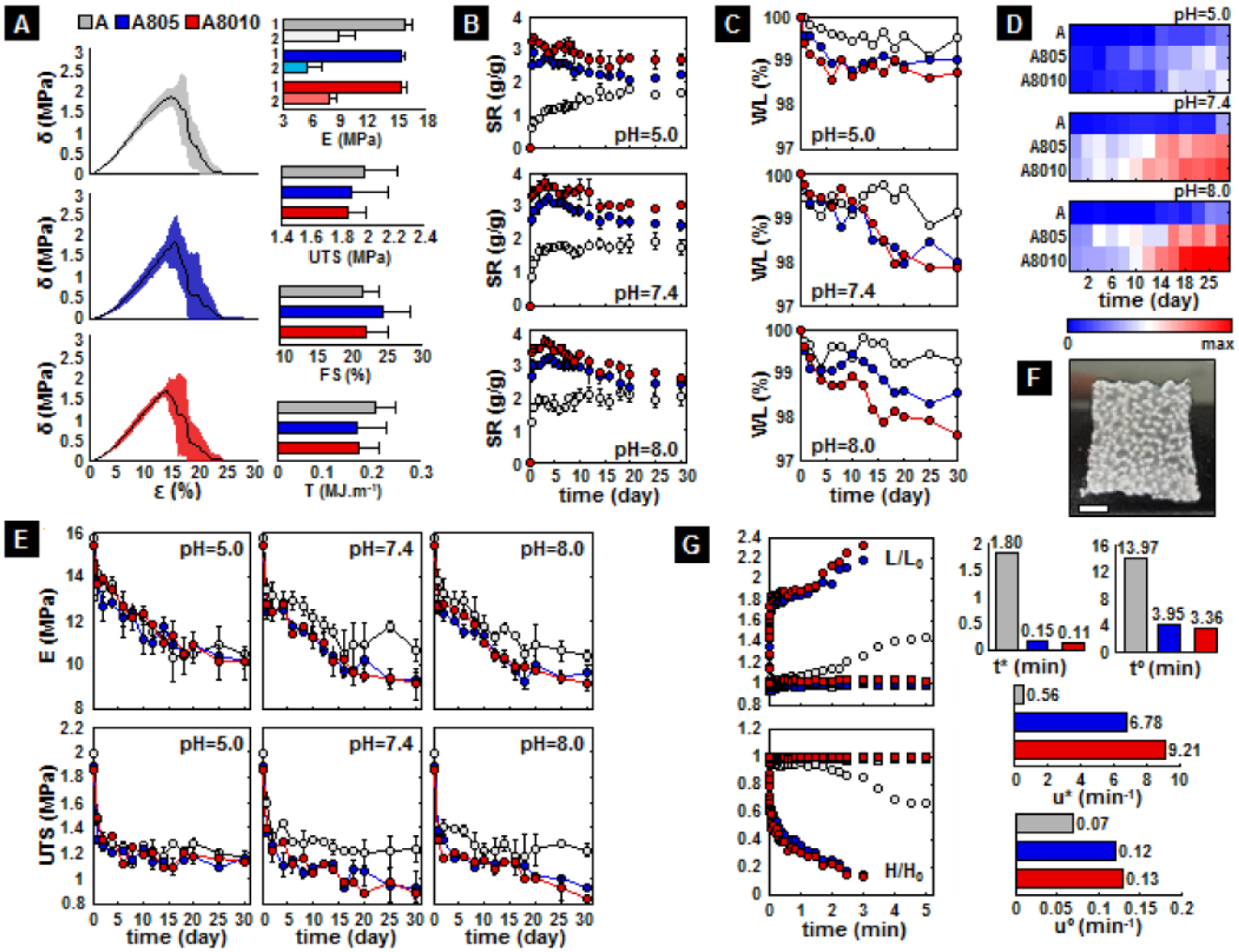

Fig. 3.

Physicochemical characterization of 3DECs. **A**, Stress(δ)-strain(ε) curves and mechanical properties determined after plasma treatment (E, Young's Modulus – 1, toe region, 2, elastic domain; UTS, Ultimate Tensile Strength; FS, Fracture Strain; T, Toughness). Time dependent swelling (**B**) and *in vitro* weight loss (**C**) as a function of pH. **D**, Cross-validation of weight loss by the qualitative PCL release profile, determined by UV absorbance measurements at 250 nm. **E**, Time dependent mechanical properties as a function of pH. **F**, Photograph of a swelled delaminated top side 3DEC while showing the presence of protrusions (scale bar = 25mm). **G**, Spreading and absorption dynamics (L/L_0, normalized droplet base; H/H_0, normalized droplet height; □, ○, bottom and top sides respectively; t*, u*, spreading time and velocity; t°, u°, imbibition time and velocity).

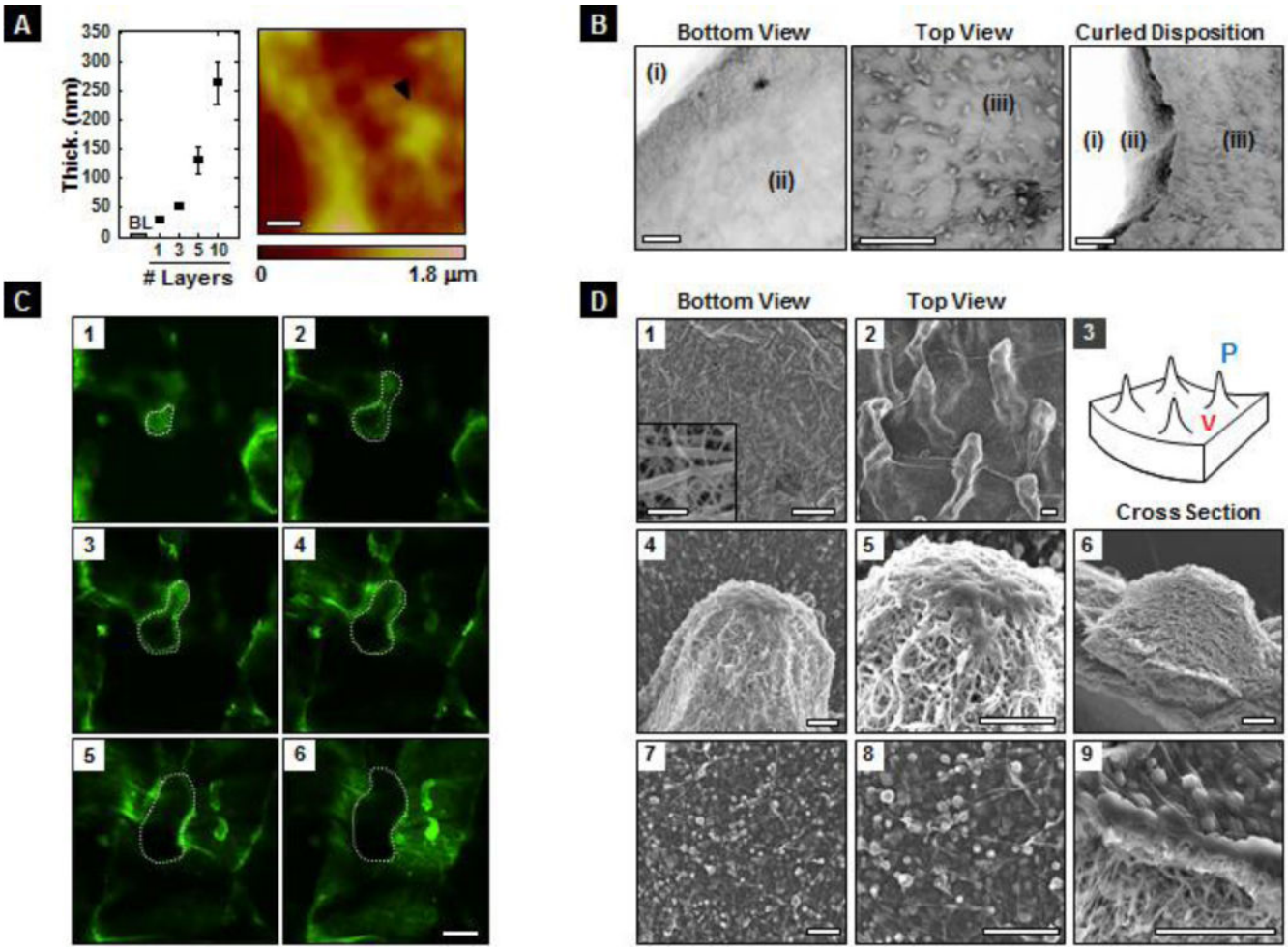

Fig. 4.

Chitosan and hyaluronic acid incorporation through spray-LbL. **A**, Film thickness growth as opposed to the number of repeated film architectures after spraying $(LPEI/DS)_{10}$ as a base layer (BL). Atomic force micrograph at 10 repeated bilayers of CHI/HA (scale bar = 5 µm). **B**, Flat-bed imaging of different 3DMECs perspectives (i, region scanned without sample; ii, bottom surface; iii, top surface; scale bar = 2 mm). **C**, Representative confocal images from a set of 33 figures with a height step of 7.17 µm, evidencing a conformal coating across the protrusion (scale bar = 2 mm). **D**, SEM images from (1) bottom, (2) top and (6,9) cross section perspectives. Images 4–6 are representative of a protrusion (P), images 7–9 are representative of an interprotrusion space (valley, V). Images 1 and 2 have a scale bar = 200 µm, where the inset scale bar in 1 = 5 µm. Images 4–9 have a scale bar = 50 µm.

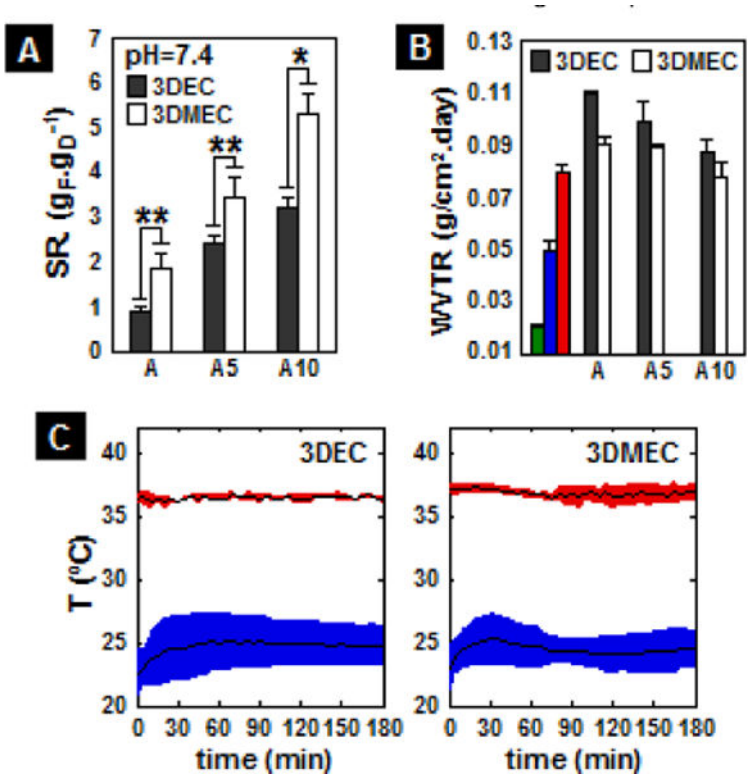

Fig. 5.

LbL-film incorporation influence in dressing properties. **A**, Swelling ratio (*, p-value < 0.01; **, p-value < 0.025). **B**, Water vapor transmission rate (Green, Normal skin; Blue, Tegaderm®; Red, OpSite®). **C**, Thermal insulation of A-type three-dimensional construct in which red stands as the wound bed temperature, and blue stands as the temperature at the constructs top side.

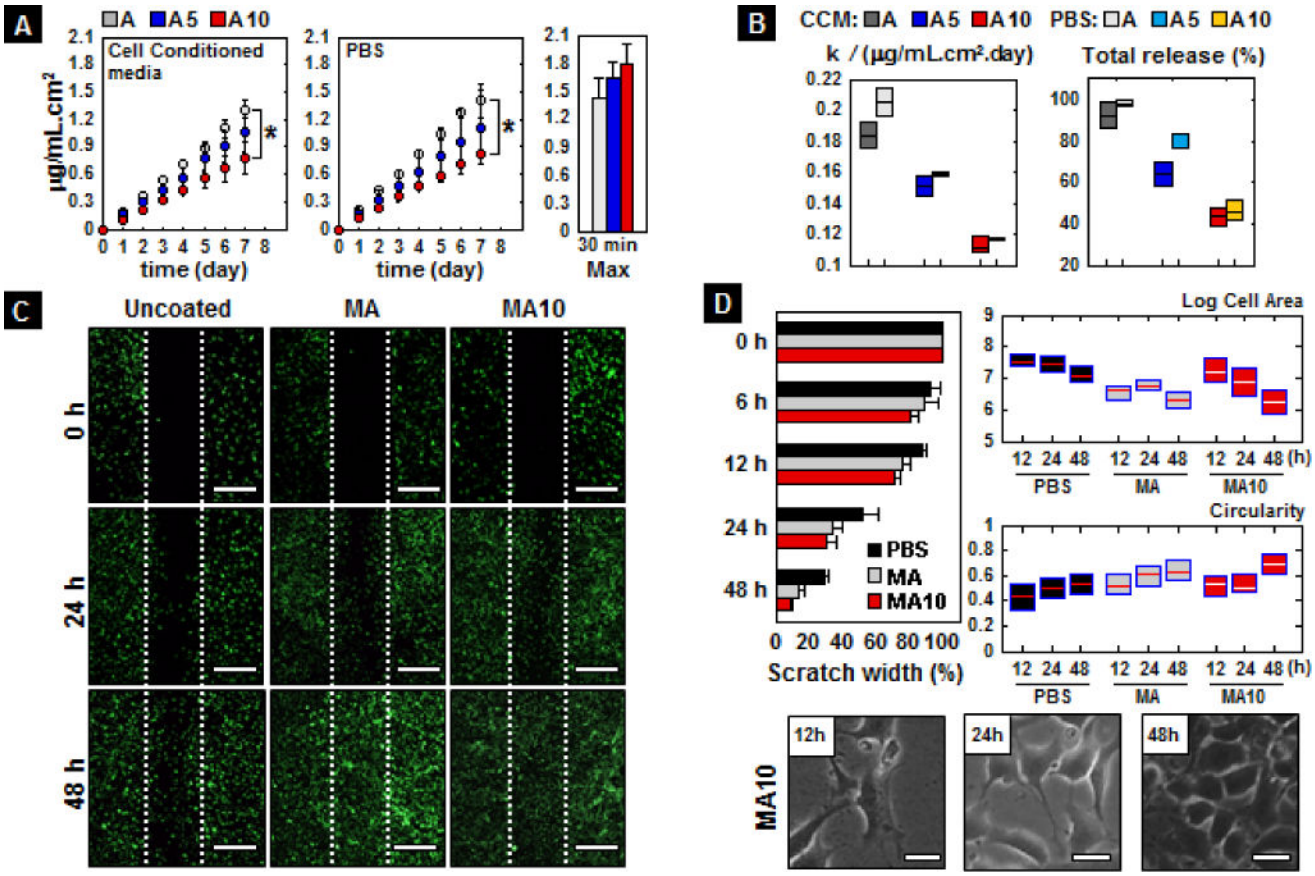

Fig. 6.

Hyaluronic acid release assessment. **A**, Hyaluronic acid release in cell conditioned media (CCM), in PBS (*, p-value < 0.025) and after sonicating samples during 30 min. **B**, Release kinetic constants (k) and total percentage of release at day 7 estimation with 95% confidence bounds. **C**, Scratch assay of uncoated, A-type and A10-type 3DMECs (scale bar = 500 μm). **D**, Gap closure dynamics and cell shape analysis at the scratch.